Physica D 240 (2011) 1574–1582

Contents lists available at SciVerse ScienceDirect

Physica D

journal homepage: www.elsevier.com/locate/physd

Wake structure of a deformable Joukowski airfoil

Adam Ysasi [a], Eva Kanso [a,*], Paul K. Newton [a,b]

[a] Department of Aerospace & Mechanical Engineering, University of Southern California, Los Angeles, CA 90089-1191, United States

[b] Department of Mathematics, University of Southern California, Los Angeles, CA 90089-1191, United States

ARTICLE INFO

Article history:
Available online 12 October 2011

Keywords:
Swimming
Vortex shedding
Unsteady point vortex

ABSTRACT

We examine the vortical wake structure shed from a deformable Joukowski airfoil in an unbounded volume of inviscid and incompressible fluid. The deformable airfoil is considered to model a flapping fish. The vortex shedding is accounted for using an unsteady point vortex model commonly referred to as the Brown–Michael model. The airfoil's deformations and rotations are prescribed in terms of a Jacobi elliptic function which exhibits, depending on a dimensionless parameter m, a range of periodic behaviors from sinusoidal to a more impulsive type flapping. Depending on the parameter m and the Strouhal number, one can identify five distinct wake structures, ranging from arrays of isolated point vortices to vortex dipoles and tripoles shed into the wake with every half-cycle of the airfoil flapping motion. We describe these regimes in the context of other published works which categorize wake topologies, and speculate on the importance of these wake structures in terms of periodic swimming and transient maneuvers of fish.

1. Introduction

The vortical wake shed from a deformable Joukowski airfoil is considered as a simple model for the wake generated by a periodically swimming fish. Our main objective is to understand the dependence of the wake structure on the airfoil motion. A characterization of the wake structure as a function of shape deformations is relevant in many applications, such as understanding the physics of fish swimming and bird flying and translating this knowledge into engineering solutions in the form of biologically-inspired underwater and airborne vehicles. For experimental studies of the wake structure see, for example, [1–3] for swimming fish, [4] for flying birds, and [5–10] for oscillating rigid foils and cylinders.

In the mathematical modeling of swimming at large Reynolds numbers due to transverse flapping such as the swimming of carangiform and anguilliform fish, different approaches have been proposed to account for the wake dynamics. In the classical work of Wu on the swimming of a deformable plate [11], the author used the assumption of small shape amplitudes which enables one to solve analytically for the trailing vortex sheet. The vortex sheet is a surface across which the tangential component of the fluid velocity is discontinuous but the normal component is continuous. Lighthill, in his slender body theory, avoided solving for the complex wake dynamics altogether by considering the momentum balance in a control volume containing the deformable body and bounded by a plane attached at its trailing edge; see for example [12]. Childress later improved on Lighthill's theory by providing an analytic approach to estimate the vorticity shed at the trailing edge [13]. Weihs modified Lighthill's theory – which focused on steady swimming – for applications to transient maneuvers and approximated the wake using classical methods of unsteady aerodynamics in terms of pre-tabulated lift and drag coefficients; see [14,15]. Lighthill's reactive force theory is revisited in [16] and the wake of a deformable body is modeled using discrete point vortices introduced manually, so-to-speak, every half cycle of the body flapping motion. In [17,18], the vortex sheet shed from the trailing edge of a deformable Joukowski airfoil is modeled using discrete point vortices with a new point vortex introduced at every time step to satisfy the Kutta–Joukowski regularity condition at the trailing edge. Resolving the dynamics of a vortex sheet shed from a deformable body is quite challenging even for prescribed or zero motion of the body; see [19–21]. Direct numerical simulations of the Navier–Stokes equations have also been used to resolve the wake dynamics; see for example [22–24].

In this work, we consider a Joukowski airfoil with prescribed shape deformations and prescribed locomotion in the form of a uniform translational velocity and periodically-varying orientation. We follow the work of [25,26] in that we model the wake using an unsteady point vortex model, also referred to as the Brown–Michael model. This model consists of introducing vorticity in the flow as point vortices of time-varying strength so that the Kutta–Joukowski regularity condition is satisfied at the sharp edge of the body; for more details, see [25,26] and the references therein.

* Corresponding author. Tel.: +1 213 821 5788.
E-mail address: Kanso@usc.edu (E. Kanso).

0167-2789/$ – see front matter © 2011 Elsevier B.V. All rights reserved.
doi:10.1016/j.physd.2011.06.021

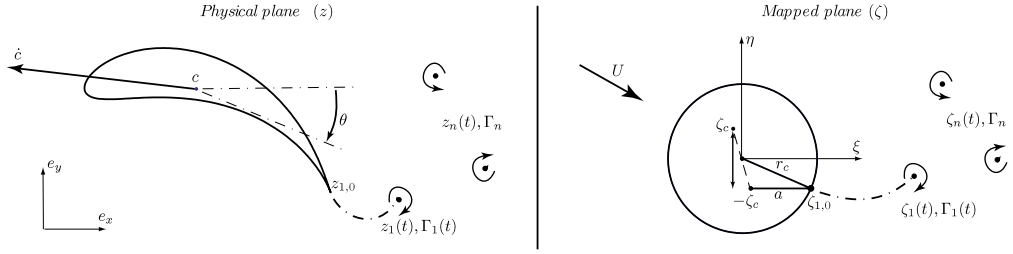

Fig. 1. Kutta–Joukowski transformation: (left) physical plane and (right) circle plane.

Roughly speaking, the unsteady point vortex model is a low-order representation of the roll-up of the vortical wake shed from the sharp edge due to boundary layer separation in a real fluid environment. Since it is physically impossible to unroll the shed wake and therefore, in the unsteady vortex model, the magnitude of the strength of the unsteady vortex is required to be monotonically increasing. That is to say, once the strength of the unsteady vortex reaches an extremum, it is kept at that value and a new unsteady vortex is started from the sharp edge. A comparison of the vortex wakes behind oscillating plates based on the Brown–Michael model, a vortex sheet model and direct numerical simulations of the full Navier–Stokes equations is reported in [27]. Interestingly, the simpler Brown–Michael model provides good approximations of the wake structure and the strength of the shed vorticity.

A review of the dynamics of N (finite and real) point vortices of constant strengths can be found in [28]. For the dynamic interaction of a rigid body with N point vortices of constant strengths, the reader is referred to [29–32] and the references therein. The coupling of the latter body-vortex system to the unsteady point vortex was first proposed in [26].

The outline of this paper is as follows. First, we prescribe periodic shape deformations of a Joukowski airfoil and assume that these prescribed deformations result in a uniform translational velocity and periodically-varying orientation of the airfoil. We then focus attention on the wake structure and its evolution in time. In particular, we examine the wake structure for a class of prescribed motions in terms of a Jacobi elliptic function which exhibits, depending on a dimensionless parameter m, a range of periodic behaviors from sinusoidal to impulsive flapping. This periodic flapping motion can also be characterized by the Strouhal number St defined as the ratio of the distance between the tip-to-tip transverse motion of the trailing edge times the frequency of flapping to the translational velocity of the airfoil. Depending on m and St, one can identify five distinct wake structures, ranging from arrays of isolated point vortices to vortex dipoles and tripoles shed into the wake with every half-cycle of the airfoil flapping motion. This categorization is compared with known published work in other settings.

2. Problem setting

Consider a uniform and neutrally-buoyant planar body $\mathcal{B}$, assumed to represent a cross-section of a fish body or fin, moving in an unbounded domain of incompressible, inviscid fluid $\mathcal{F}$ at rest at infinity. For concreteness, let $\mathcal{B}$ take the form of a Joukowski airfoil whose boundary can be conformally mapped to a circle of radius r_c. We introduce an orthonormal inertial frame $\{\mathbf{e}_{1,2,3}\}$ where the directions $\{\mathbf{e}_1, \mathbf{e}_2\}$ span the physical plane of motion and $\mathbf{e}_3$ is the unit normal to this plane. The orientation of $\mathcal{B}$ can be described by the rotation angle θ about $\mathbf{e}_3$ and its location can be specified by the coordinates of its centroid $c \equiv (c_1, c_2)$ in the $(\mathbf{e}_1, \mathbf{e}_2)$ plane; see Fig. 1. It is more convenient for what follows to introduce the complex variable $z = x + \mathrm{i}y$ (where $\mathrm{i} = \sqrt{-1}$) and its complex conjugate $\bar{z} = x - \mathrm{i}y$. It is also convenient to parameterize the circle plane by the complex variable $\zeta = \xi + \mathrm{i}\eta$, measured from a fixed point O located at the center of the circle. The conformal transformation from the physical plane to the circle plane can be written in the general form (see, e.g., [26])

$$z = c + g(\zeta)\mathrm{e}^{\mathrm{i}\theta}, \tag{1}$$

where the mapping $g(\zeta)$ is given by

$$g(\zeta) = \zeta + \zeta_c + \frac{a^2}{\zeta + \zeta_c}. \tag{2}$$

The parameters a and $\zeta_c = \xi_c + \mathrm{i}\eta_c$ determine the shape of the airfoil (see, e.g., [18]), and the radius of the circle r_c depends on a and ζ_c as follows

$$r_c^2 = (a - \xi_c)^2 + \eta_c^2. \tag{3}$$

We prescribe shape deformations of the airfoil by varying the position of $\zeta_c(t)$ as a function of time t while maintaining the radius of the circle r_c constant which means that a also varies in order to satisfy (3). In particular, we consider deformations of the form

$$\zeta_c = \xi_o + \mathrm{i}\eta_c(t), \tag{4}$$

where ξ_o is non-zero constant and $\eta_c(t)$ varies periodically as depicted in Fig. 1. These prescribed deformations are not area preserving in general. That is to say, the area of the airfoil $A = \frac{1}{2\mathrm{i}}\int \bar{z}\mathrm{d}z$ varies in time. However, for all examples considered in this paper, the deviations from constant are quite small, $\Delta A/A_o \approx 0.01$ where A_o is the airfoil area at time $t = 0$.

As the airfoil deforms, the location of its centroid in the physical plane changes. The centroid position c is dictated by both the prescribed deformations and the orientation θ of the airfoil such that

$$c = -z_c\mathrm{e}^{\mathrm{i}\theta}, \tag{5}$$

where z_c is defined by $Az_c = -\frac{1}{4\mathrm{i}}\int z^2\overline{\mathrm{d}z}$. When expressed as function of the prescribed deformations $\zeta_c(t)$ (and in turn $a(t)$) in the circle plane, one has

$$z_c = \frac{a^6\bar{\zeta}_c + \zeta_c(r_c^2 - \zeta_c\bar{\zeta}_c)^3}{(r_c^2 - \zeta_c\bar{\zeta}_c)[(r_c^2 - \zeta_c\bar{\zeta}_c)^2 - a^4]}. \tag{6}$$

We assume that the prescribed cyclic deformations induce a uniform translational velocity (V_x, V_y) and a periodic rotational velocity $\omega(t) = \dot{\theta}(t)$ of the airfoil in the physical plane. In other words, we do not solve the coupled body-fluid system to obtain the locomotion of the airfoil due to the prescribed deformations as done in [33,16]. Rather, we impose on the airfoil a net locomotion consisting of a steady translation and periodic rotations. To this end, the velocity of the centroid is given by

$$v_c = (V_x + \mathrm{i}V_y) - (\dot{z}_c - \mathrm{i}\omega z_c)\,\mathrm{e}^{\mathrm{i}\theta}. \tag{7}$$

The resulting free stream velocity in the circle plane is

$$U = -\overline{v}_c\mathrm{e}^{\mathrm{i}\theta} = \dot{\bar{z}}_c - \mathrm{i}\omega\bar{z}_c - \left(V_x - \mathrm{i}V_y\right)\mathrm{e}^{\mathrm{i}\theta}. \tag{8}$$

The Joukowski airfoil sheds a vortical wake from its sharp edge as it deforms in the fluid domain. We account for the shed

vorticity using the unsteady point vortex model which consists, as explained in Section 1, of introducing vorticity in the flow as point vortices of monotonically-varying strength so that the Kutta condition is satisfied at the sharp edge; see [25,26]. For concreteness, the unsteady vortex is identified by its variable strength $\Gamma_1(t)$ and location $z_1(t)$ while the previously shed point vortices have frozen strengths $\Gamma_2, \ldots, \Gamma_N$ and time-dependent positions $z_2(t), \ldots, z_N(t)$.

3. Fluid velocity and complex potential

The complex potential function is defined as $F(z) = \phi(x, y) + \mathrm{i}\psi(x, y)$, with ϕ being the real potential function and ψ the stream function. The existence of ϕ and ψ is guaranteed by irrotationality (except at the location of the point vortices) and by the continuity equation $\mathrm{div}(u) = 0$, respectively; see for example [34]. By linearity of the problem, the complex potential $F(z)$ can be written as a superposition of the contributions $F_b(z)$ due to translational and rotational velocities of the airfoil, $F_s(z)$ due to shape deformations and $F_n(z)$ due to the presence of point vortices in the wake,

$$F(z) = F_b(z) + F_s(z) + \sum_{n=1}^{N} \Gamma_n F_n(z). \tag{9}$$

The potential F_b due to the rigid motion of the airfoil is harmonic in the fluid domain with proper decay at infinity while satisfying the boundary conditions on the airfoil surface C

$$Re\left[-\mathrm{i}F_b\right]_C = Re\left[-\mathrm{i}\bar{v}_c(z-c) - \frac{1}{2}\omega|z-c|^2\right]. \tag{10}$$

That is, $F_b(z)$ has the form of a Riemann–Hilbert problem (see, e.g., [35,36]) and it can be transformed, using the conformal mapping (1) and its inverse, into a Dirichlet problem in the circle plane whose solution is given in terms of the Schwarz formula. To this end, one gets

$$F_b(\zeta) = U(\zeta - g(\zeta)) + \frac{r_c^2}{\zeta}\bar{U} - \mathrm{i}\omega r, \tag{11}$$

where

$$r(\zeta) = \frac{1}{2}\left(r_c^2 + 2\zeta_c\frac{r_c^2}{\zeta} + \zeta_c\bar{\zeta}_c + \frac{2a^2\left(r_c^2 + \zeta\bar{\zeta}_c\right)}{\zeta\,(\zeta+\zeta_c)} + \frac{a^4(\zeta-\zeta_c)}{(\zeta+\zeta_c)(r_c^2 - \zeta_c\bar{\zeta}_c)}\right). \tag{12}$$

The complex potential due to body deformations is constructed as a linear superposition of the two components,

$$F_s(\zeta) = F_\eta(\zeta)\dot{\eta}_c + F_a(\zeta)\dot{a}. \tag{13}$$

F_η and F_a are also harmonic in the fluid domain with proper decay at infinity while satisfying the following boundary conditions at the airfoil surface C and the circle surface Σ

$$Re\left[-\mathrm{i}\frac{\mathrm{d}F_\eta}{\mathrm{d}\zeta}\mathrm{d}\zeta\right]_\Sigma = Re\left[-\mathrm{i}\overline{\frac{\partial g(\zeta)}{\partial \eta_c}}\mathrm{d}z\right]_C,$$
$$Re\left[-\mathrm{i}\frac{\mathrm{d}F_a}{\mathrm{d}\zeta}\mathrm{d}\zeta\right]_\Sigma = Re\left[-\mathrm{i}\overline{\frac{\partial g(\zeta)}{\partial a}}\mathrm{d}z\right]_C. \tag{14}$$

Upon integrating both sides of (14) for F_η and F_a and ensuring that Kelvin's conservation of circulation around the airfoil is satisfied (see [18] for more details), one gets that

$$\begin{aligned}
F_\eta(\zeta) &= -\mathrm{i}\left[-\frac{r_c^2}{\zeta} + \frac{a^2r_c^2}{\zeta\zeta_c^2} + \frac{a^2}{\rho} - \frac{a^4\zeta_c^2}{\rho\delta^4} - \frac{2a^4r_c^2\zeta_c}{\delta^6}\log\left(\frac{\rho}{r_c}\right) - \left(\frac{a^2r_c^2}{\zeta_c^3} - \frac{a^4r_c^2}{\zeta_c\delta^4}\right)\frac{\zeta}{\rho}\right.\\
&\quad + 2a^2r_c^2\left(\frac{1}{\zeta_c^3} + \frac{\bar{\zeta}_c a^2}{\delta^6}\right)\log\left(\frac{\rho}{\zeta}\right)\\
&\quad \left. + \frac{2a^4r_c^2\zeta_x}{\delta^6}\log\left(\frac{\zeta}{r_c}\right)\right],\\
F_a(\zeta) &= 2a\left(-\frac{r_c^2}{\zeta\zeta_c} - \frac{a^2\zeta_c}{\rho\delta^2} - \frac{a^2r_c^2}{\delta^4}\log\left(\frac{\rho}{r_c}\right)\right.\\
&\quad \left. + \frac{r_c^2(\delta^4 - a^2\zeta_c^2)}{\zeta_c^2\delta^4}\log\left(\frac{\rho}{\zeta}\right)\right),
\end{aligned} \tag{15}$$

where $\rho = \zeta + \zeta_c$ and $\delta^2 = r_c^2 - \zeta_c\bar{\zeta}_c$.

The complex potential due to the presence of N point vortices is given by the well-known Milne–Thomson theorem (also known as the circle theorem; see [37])

$$F_n(\zeta) = \frac{1}{2\pi\mathrm{i}}\left[\log(\zeta - \zeta_n) - \log\left(\zeta - \frac{r_c^2}{\bar{\zeta}_n}\right)\right], \tag{16}$$

where $r_c^2/\bar{\zeta}_n$ is the position of the image vorticity.

The complex fluid velocity $\bar{u} = u_x - \mathrm{i}u_y$ at a point $z = x + \mathrm{i}y$ in the physical plane that does not coincide with a point vortex is obtained from the relation

$$\bar{u} = \frac{\mathrm{d}F(z)}{\mathrm{d}z} = \frac{\mathrm{d}F(z(\zeta))}{\mathrm{d}\zeta}\frac{\mathrm{d}\zeta}{\mathrm{d}z}, \tag{17}$$

whereas, due to a theorem by Lin [38,39], the regularized velocity induced at a point vortex z_n is given by

$$\bar{u}_n = \frac{\mathrm{d}}{\mathrm{d}z}\left[F(z) - \frac{\Gamma_n}{2\pi\mathrm{i}}\log(z - z_n)\right]_{z_n}. \tag{18}$$

In particular, Eq. (17) takes the form

$$\bar{u} = \bar{v}_c + \frac{\mathrm{e}^{-\mathrm{i}\theta}}{g'(\zeta)}\left[U - \frac{r_c^2}{\zeta^2}\bar{U} - \mathrm{i}\frac{\partial r}{\partial\zeta}\omega + \frac{\partial F_\eta}{\partial\zeta}\dot{\eta}_c + \frac{\partial F_a}{\partial\zeta}\dot{a} + \sum_{n=1}^{N}\frac{\Gamma_n}{2\pi\mathrm{i}}\left(\frac{1}{\zeta - \zeta_n} - \frac{\bar{\zeta}_n}{\zeta\bar{\zeta}_n - r_c^2}\right)\right]. \tag{19}$$

Eq. (19) is used to compute the velocity at the trailing edge of the airfoil denoted by $\zeta_{1,0} = a - \zeta_c$, as shown in Fig. 1. It is important to observe that the velocity in (19) admits a singularity at the trailing edge $\zeta_{1,0}$. This is apparent by noting that $g'(\zeta) = \partial g/\partial\zeta = 1 - a^2/(\zeta + \zeta_c)^2$ which at $\zeta_{1,0} = a - \zeta_c$ is equal to zero. To eliminate this singularity, we impose the Kutta–Joukowski regularity condition by introducing an unsteady point vortex in the flow as mentioned in Section 2 that makes the quantity in the bracket of Eq. (19) vanish as discussed below.

4. Equations of motion

The equations of motion for the system of vortices is expressed more compactly in the physical plane and consists of the following set of $2N$ ordinary differential equations

$$\dot{z}_n + (z_n - z_{n,0})\frac{\dot{\Gamma}_n}{\Gamma_n} = \bar{u}_n, \tag{20}$$

where the complex conjugate of u_n is given by (18) and the term containing $\dot{\Gamma}_n$ is known as the Brown–Michael correction term. Here, it is non-zero only for the unsteady vortex Γ_1 and zero for

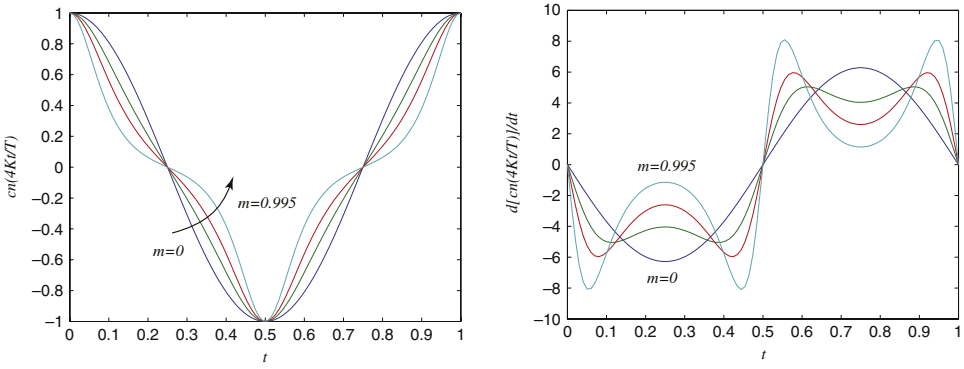

(a) $cn(4Kt/T)$. (b) d $(cn(4Kt/T))$ /dt.

Fig. 2. Plots of (a) the cnoidal function $cn(4Kt/T)$ and (b) its time derivative versus time t for $m = 0, 0.8, 0.95, 0.995$. Note that for $m = 0$, one recovers the cosine function. The period is set to $T = 1$.

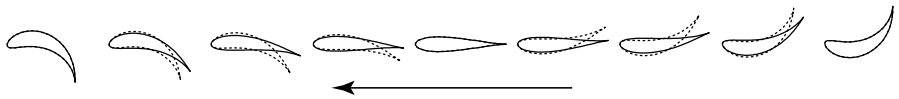

Fig. 3. Geometry of Joukowski airfoil over a half cycle $2K/T$ for prescribed flapping $\zeta_c = \xi_o + i\eta_o\, cn(4Kt/T)$ and orientation $\theta(t) = \theta_o\, cn(4Kt/T)$. The case of $m = 0$ is shown in dashed line and $m = 0.995$ in black line. The parameter values are set to $\xi_o = -1/8$ $\eta_o = -1/2$, $\theta_o = 1/2$, $r_c = 1$ and $T = 1$.

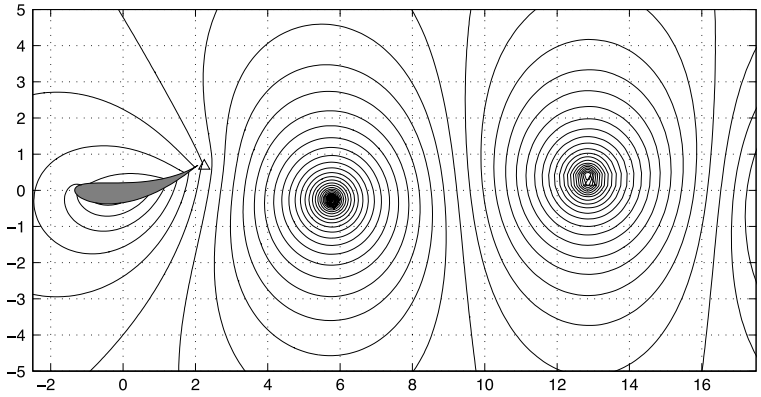

(a) streamlines.

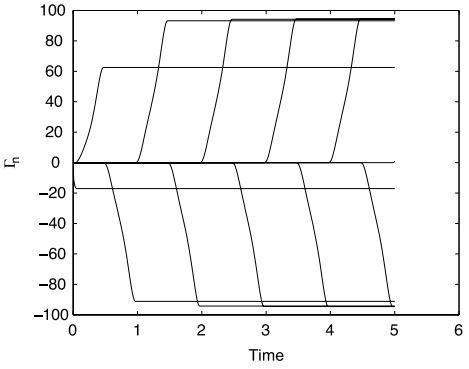

(b) Γ_n versus t.

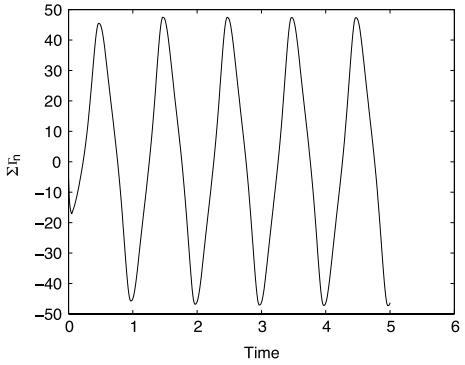

(c) $\sum \Gamma_n$ versus t.

Fig. 4. (a) Snapshot of the streamlines at $t = 5.002$, (b) strength of Γ_n versus time and (c) $\sum \Gamma_n$ versus time for prescribed motions $\zeta_c = -0.125 - \mathrm{i}0.2\, cn(4Kt/T)$, $\theta = 0.2\, cn(4Kt/T)$ and parameters $m = 0.8$ and $St = 0.1$ which correspond to Region I in Fig. 9.

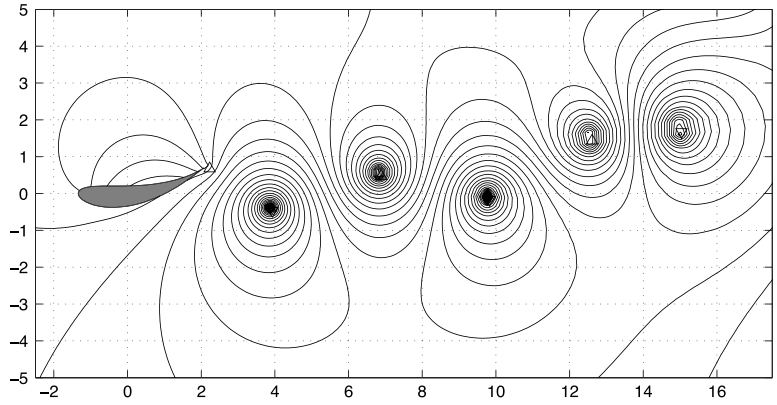

(a) streamlines.

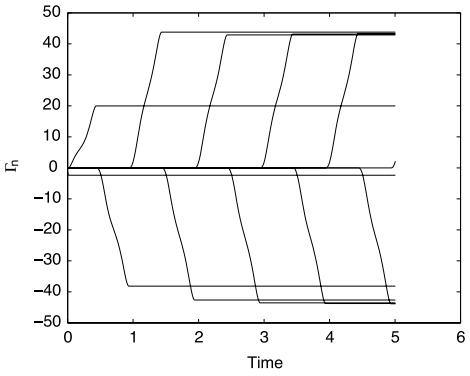

(b) Γ_n versus t.

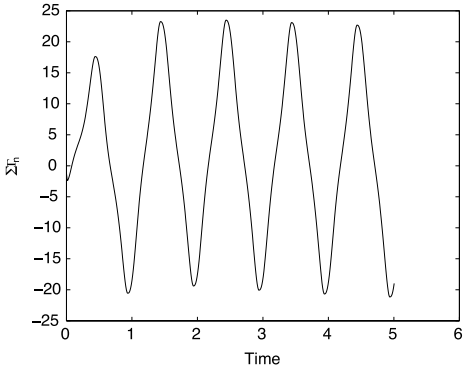

(c) $\sum \Gamma_n$ versus t.

Fig. 5. (a) Snapshot of the streamlines at $t = 5.002$, (b) strength of Γ_n versus time and (c) $\sum \Gamma_n$ versus time for prescribed motions $\zeta_c = -0.125 - \mathrm{i}0.2\,cn(4Kt/T)$, $\theta = 0.2\,cn(4Kt/T)$ and parameters $m = 0.8$ and $St = 0.3$ which correspond to Region II in Fig. 9.

all $n \geq 2$. These equations can be written in the circle plane by substituting (1) and (18) into (20). The resulting expression takes the form

$$\begin{aligned} &g'(\zeta_n)\dot{\bar{\zeta}}_n + (g(\zeta_n) - g(\zeta_{n,0}))\frac{\dot{\Gamma}_n}{\Gamma_n} \\ &= -\mathrm{i}\omega g(\zeta_n) - g'(\zeta_n)\dot{\eta}_c - \frac{\partial g(\zeta_n)}{\partial a}\dot{a} + \frac{1}{\overline{g'(\zeta_n)}} \\ &\quad\times\left[\bar{U} - \frac{r_c^2}{\bar{\zeta}_n^2}U + \mathrm{i}\omega\overline{\frac{\partial r(\zeta_n)}{\partial \zeta_n}} + \overline{\frac{\partial F_\eta(\zeta_n)}{\partial \zeta_n}}\dot{\eta}_c + \overline{\frac{\partial F_a(\zeta_n)}{\partial \zeta_n}}\dot{a}\right. \\ &\quad - \sum_{j\neq n}\frac{\Gamma_j}{2\pi\mathrm{i}}\left(\frac{1}{\bar{\zeta}_n - \bar{\zeta}_j} - \frac{\zeta_j}{\zeta_j\bar{\zeta}_n - r_c^2}\right) \\ &\quad\left. + \frac{\Gamma_n}{2\pi\mathrm{i}}\left(\frac{\zeta_n}{\zeta_n\bar{\zeta}_n - r_c^2} + \frac{\overline{g''(\zeta_n)}}{2\overline{g'(\zeta_n)}}\right)\right]. \end{aligned} \tag{21}$$

The Kutta condition is used to ensure that the complex velocity (19) remains finite at the trailing edge of the airfoil $\zeta_{1,0} = a - \zeta_c$. This amounts to evaluating the quantity in the bracket at $\zeta_{1,0}$ and setting it to zero, which upon some simplifications gives

$$\begin{aligned} &2Im\left(U\zeta_{1,0}\right) - \omega\zeta_{1,0}r_1' - \mathrm{i}\zeta_{1,0}\left(u_{\eta,0}\dot{\eta}_c + u_{a,0}\dot{a}\right) \\ &\quad + \sum_{n=1}^{N}\frac{\Gamma_n}{2\pi}\left(1 + 2Re\left(\frac{\zeta_{1,0}}{\zeta_n - \zeta_{1,0}}\right)\right) = 0, \end{aligned} \tag{22}$$

where

$$r_1' = \left.\frac{\partial r}{\partial \zeta}\right|_{\zeta=\zeta_{1,0}}, \qquad u_{\eta,0} = \left.\frac{\partial F_\eta}{\partial \zeta}\right|_{\zeta=\zeta_{1,0}},$$

$$u_{a,0} = \left.\frac{\partial F_a}{\partial \zeta}\right|_{\zeta=\zeta_{1,0}}. \tag{23}$$

Eqs. (21) and (22) form an algebraic-differential set of $2N + 1$ equations which we solve for $\Gamma_1(t)$ and $z_n(t)$, $n = 1, \ldots, N$.

It is important to note here that this system of equations is ill-posed when a new unsteady vortex is started from the trailing edge because the right-hand side of (21) is singular. Indeed, at the onset of shedding, the vortex and its image conjugate are at the same point. To overcome this difficulty, we follow the approach in [25,40,26] and propose an analytic solution valid only for small time which we use to obtain the initial behavior of the system; see Appendix for details.

5. Wake structure

In this section, we study the behavior of the wake as a function of the prescribed deformations and prescribed translational and rotational motions of the airfoil. We particularly examine prescribed deformations, orientation and translational velocities of the Joukowski airfoil of the form

$$\begin{aligned} &\zeta_c = \xi_o + i\eta_o\,cn\left(\frac{4K}{T}t\right), \qquad \theta = \theta_o\,cn\left(\frac{4K}{T}t\right), \\ &V_x = V_o, \qquad V_y = 0. \end{aligned} \tag{24}$$

Here, ξ_o, η_o, θ_o and V_o are non-zero constants and $cn(4Kt/T)$ is the cnoidal elliptic function with $K(m)$ given by $K(m) = \int_0^{\pi/2} \mathrm{d}\phi/(1 - m\sin^2\phi)^{1/2}$ and T the period of flapping or shape cycle. It is worth noting that m is a dimensionless parameter that determines the profile of the cnoidal function as shown in Fig. 2. If $m = 0$, one

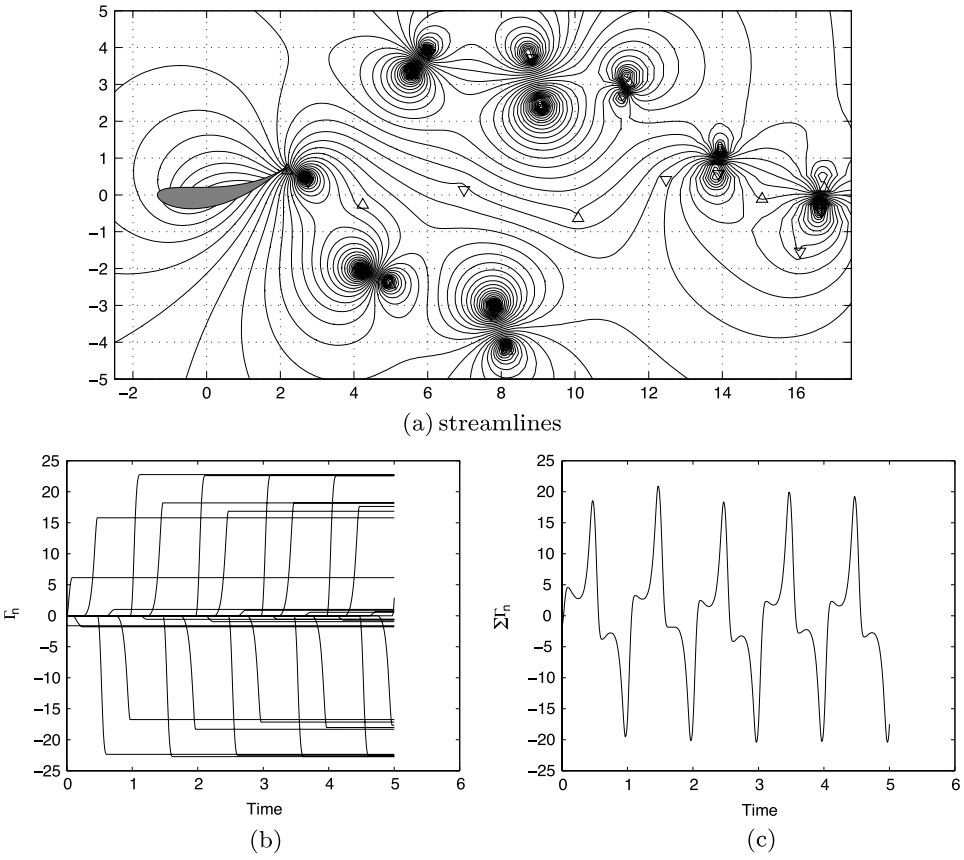

Fig. 6. (a) Snapshot of the streamlines at $t = 5.002$, (b) strength of Γ_n versus time and (c) $\sum \Gamma_n$ versus time for prescribed motions $\zeta_c = -0.125 - \mathrm{i}0.2\,cn(4Kt/T)$, $\theta = 0.2\,cn(4Kt/T)$ and parameters $m = 0.995$ and $St = 0.3$ which correspond to Region IV in Fig. 9.

recovers the sinusoidal cosine function $\cos(2\pi t/T)$ and if $m = 1$, one gets the hyperbolic secant. Note that as m increases, the time derivative of the cnoidal function (shown in Fig. 2(b)) changes rapidly when the airfoil reaches its maximum, zero and minimum flapping angles. It is this rapid change in the shape deformations that we refer to as impulsive flapping. The airfoil motion in the physical plane is illustrated in Fig. 3 for two parameter values $m = 0$ and $m = 0.995$. This motion can be characterized by two parameters: m which dictates the shape of the cnoidal function as depicted in Fig. 2 and the Strouhal number St defined as

$$St = \frac{L}{V_o T}. \tag{25}$$

In (25), the length scale L is defined by the lateral motion of the trailing edge. Our objective is to map out the dependence of the wake structure on the Strouhal number St and the dimensionless parameter m which dictates the profile of the periodic deformations, from sinusoidal to impulsive.

The conformal mapping approach presented in this paper transforms the problem of wake generation behind the deforming airfoil into that of vortex formation behind a cylinder oscillating in a free stream. Vortex formation behind a cylinder oscillating in a free stream is a classical example that is known to afford a great variety of wake structures depending on the cylinder's oscillations; see the seminal work of Williamson & Roshko in [10]. Williamson and Roshko mapped out the wake structures behind the oscillating cylinder as function of the oscillation parameters, namely, the amplitude and frequency (or Strouhal number) of the harmonic oscillations. A simple mathematical model was later developed in [41] to explain the important wake transitions. Examples of the wakes reported in [10] include von Kármán-type wakes, referred to as 2S wakes, in which two vortices of opposite sign are shed per oscillation period and 2P wakes in which two vortex pairs are shed per oscillation period. We use this terminology to categorize the wake structures obtained here in the context of the simplified Brown–Michael vortex model.

It is worth noting that the idea of mapping out the dependence of the wake structure on the oscillation parameters was recently reconsidered in [8] for a symmetric rigid airfoil oscillating in a two-dimensional free stream created by a vertically flowing soap film. These soap-film experiments focused on sinusoidal pitching oscillations and reported a wide variety of simple and exotic wakes for various amplitude and frequency of oscillations. The focus of our study, as mentioned earlier, is to understand the dependence of wake structure on the swimming velocity (as reflected by Strouhal number St) and the profile of the periodic deformations, from sinusoidal to impulsive (as dictated by the dimensionless parameter m).

In Figs. 4–8, we show the wake structure obtained by varying the parameters m and St while the remaining parameters are held at $\eta_o = -1/5$, $\xi_o = -1/8$, $\theta_o = 1/5$, $r_c = 1$, and $T = 1$. In other words, the Strouhal number St is varied by varying the translational velocity V_o. Panels (a) in Figs. 4–8 show snapshots of the streamlines of the velocity field at $t = 5.002$ while panels (b) and (c) show the strength of the shed vortices and the total circulation in the wake (sum of strength) versus time, respectively. Each of these figures represent one of five distinct structures of the wake that we identified depending on the two parameters m and St; see Fig. 9. The results in Fig. 9 are obtained by discretizing the parameter space (St, m) and computing the wake of the deformable airfoil at each of these discrete points. In region I where the Strouhal number is low $St < 0.2$, that is to say, the translational velocity V_o is large, the wake, after some transient behavior, is an aligned 2S wake that resembles an array of

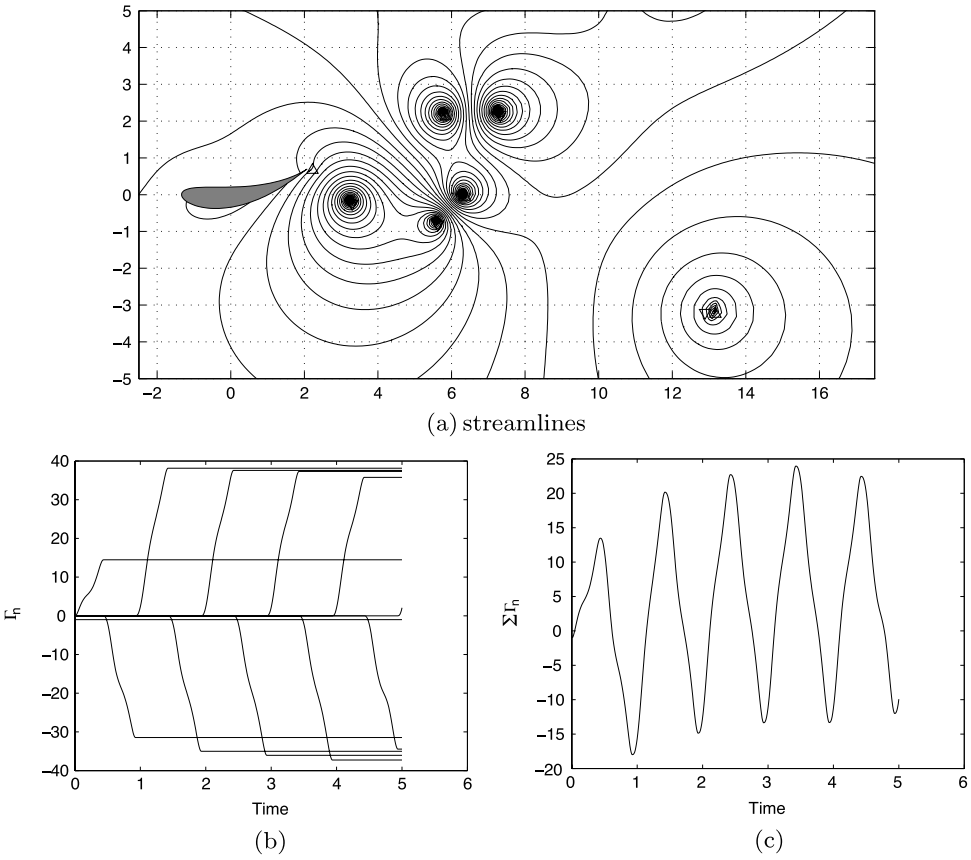

Fig. 7. (a) Snapshot of the streamlines at $t = 5.002$, (b) strength of Γ_n versus time and (c) $\sum \Gamma_n$ versus time for prescribed motions $\zeta_c = -0.125 - \mathrm{i}0.2\,cn(4Kt/T)$, $\theta = 0.2\,cn(4Kt/T)$ and parameters $m = 0.8$ and $St = 0.5$ which correspond to Region III in Fig. 9.

isolated point vortices of equal and opposite circulations, with two vortices of equal and opposite strength shed per oscillation period as evidenced in Fig. 4.

As the Strouhal number increases $0.2 < St < 0.4$, the structure of the wake bifurcates depending on the value m: in region II for $m < 0.95$ the wake structure is similar to a reverse von Kármám wake or 2S wake (Fig. 5) whereas in region IV for $m > 0.95$, that is to say, for impulsive motion, one gets a 2P wake with predominantly two point vortices shed in every half cycle of the airfoil oscillations and pair-up to form vortex dipoles that propagate obliquely in the flow (Fig. 6), with their direction being determined by initial conditions. The increased shedding periodicity is evident in Fig. 6(b). Numerically, three vortices are shed each half-cycle where one vortex has negligible effect given that its intensity is much smaller than the other two (see Fig. 6(b) and (c)).

As the Strouhal number increases further $0.4 < St < 0.6$, the von Kármám structure observed in region II disappears as the vortices shed in two consecutive cycles of oscillations begin to pair-up and propagate obliquely as dipoles resulting in a P wake (Fig. 7). Finally, the dipoles shed every half cycle of oscillations in region IV are now replaced by tripoles also shed every half-cycle of oscillations as evidenced in Fig. 8(b) and (c). More specifically, the previously negligible vortex in region IV now has significantly higher strength, resulting in what initially sheds as a 2P + 2S wake. Due to downstream vortex interactions, the wake structure breaks up into tripoles and more complex configurations.

6. Conclusions

A deformable Joukowski airfoil is proposed as a model for the flapping of a fish body or tail in an otherwise quiescent fluid. The wake structure is investigated as a function of m and St where m indicates the profile of the flapping motion, from smooth sinusoidal motion to more sharply peaked, but still periodic motion. The Strouhal number St indicates the ratio of the flapping speed to the translational motion of the fish. For almost sinusoidal flapping $m < 0.95$ in the range $0.2 < St < 0.4$, which is the range of Strouhal numbers identified in the experimental work [3] as the optimal range in terms of swimming efficiency, we find that the wake structure corresponds to a reverse von Kármán street. For lower St, the wake structure consists of an array of isolated point vortices with no fluid jet propagating downstream. This wake structure presents little advantage to the flapping airfoil in terms of momentum thrust induced by the wake. For higher St, the point vortices shed in two consecutive cycles of flapping begin to pair-up to form vortex dipoles that propagate obliquely to the direction of motion, also reducing the locomotory advantage of a thrust wake. For impulsive flapping $m > 0.95$, we find that as the Strouhal number increases, the airfoil begins to shed three point vortices with every half-cycle of its flapping motion. For $0.2 < St < 0.4$, the third vortex shed when the airfoil approaches its straight-out configuration has negligible magnitude and the wake structure consists of dipoles shed every half-cycle of flapping. For $0.4 < St < 0.6$, the third vortex becomes stronger and pairs with the other two point vortices to form a tripole shed every half-cycle of flapping. We conjecture that these sharper flapping strokes are more suited for transient turning maneuvers than for steady swimming, and that the net mean force on the body becomes zero in the region $St < 0.2$. Future extensions of this work will include computing the forces and moments acting on the airfoil and solving for the coupled body-wake time evolution with application to transient maneuvers. The resulting wakes will be compared with reported experimental and numerical data on fish wakes such as in [22,2].

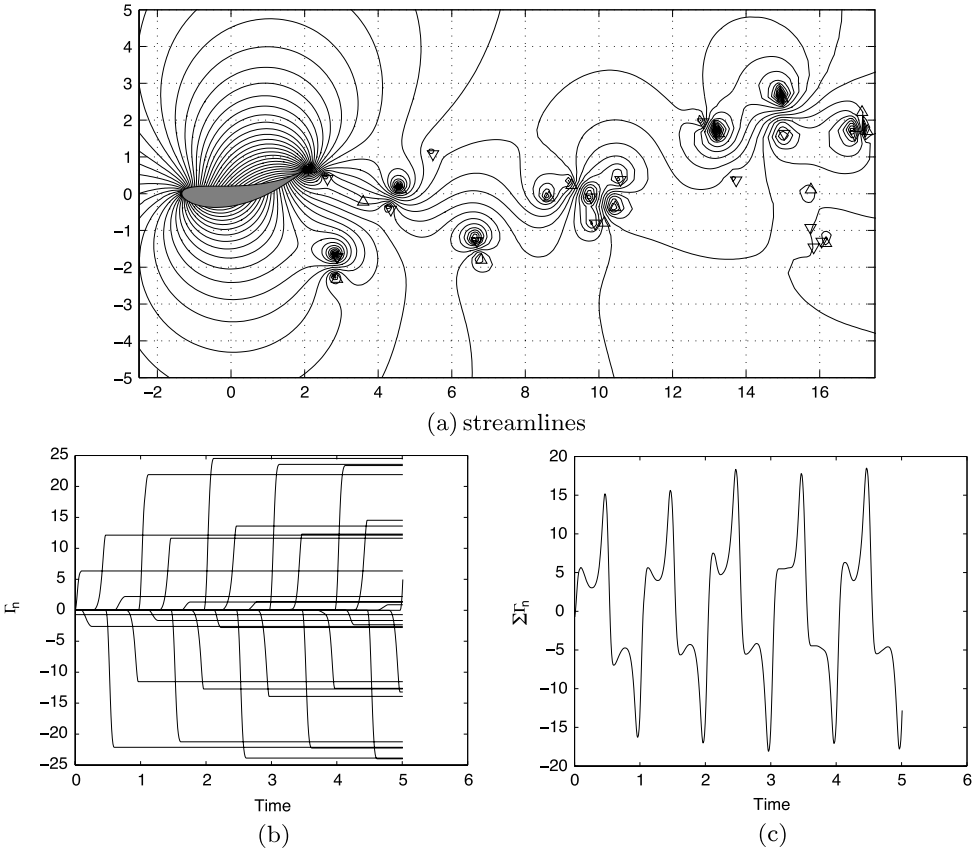

Fig. 8. (a) Snapshot of the streamlines at $t = 5.002$, (b) strength of Γ_n versus time and (c) $\sum \Gamma_n$ versus time for prescribed motions $\zeta_c = -0.125 - \mathrm{i}0.2\,cn(4Kt/T)$, $\theta = 0.2\,cn(4Kt/T)$ and parameters $m = 0.995$ and $St = 0.5$ which correspond to Region V in Fig. 9.

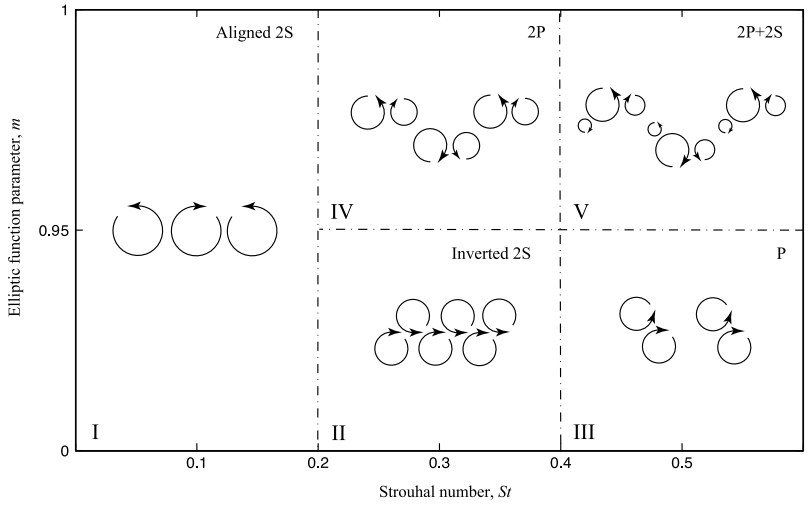

Fig. 9. Wake structure as a function of the two dimensionless parameters m and St.

Acknowledgments

The work of A.Y. and E.K. is partially supported by the National Science Foundation through the CAREER award CMMI 06-44925 and the grant CCF 08-11480.

Appendix. Onset of vortex shedding

Vorticity is generated by the motion of the sharp trailing edge of the airfoil. At the time a new vortex is started, one gets a singularity at the trailing edge. It is therefore necessary to use small-time analysis to solve for the initial behavior. The small time analysis is based on the system of Eqs. (21) and (22) in the mapped plane. Defining ϵ such that $\zeta_1 = \zeta_{1,0}(1+\epsilon)$, the Kutta condition (22) then becomes:

$$2Im(U\zeta_{1,0}) - \omega\zeta_{1,0}r_1' - \mathrm{i}\zeta_{1,0}\left(u_{\eta,0}\dot{\eta}_c + u_{a,0}\dot{a}\right) + \frac{\Gamma_1}{\pi}Re\left(\frac{1}{\epsilon}\right) + \sum_{n=2}^{N}\frac{\Gamma_n}{2\pi}\left[1 + 2Re\left(\frac{\zeta_{1,0}}{\zeta_n - \zeta_{1,0}}\right)\right] = 0. \quad \text{(A.1)}$$

The Taylor series expansion of (21) is taken about $\zeta_{1,0}$. Keeping only the dominant terms produces the following, with $\tau = t - t_s$ and t_s

the time of shedding:

$$\zeta_{1,0}^2 g_1'' \left(\epsilon\dot{\epsilon} + \frac{5\epsilon^2}{4\tau}\right) = -\mathrm{i}\omega g_1 - 2\dot{a} + \frac{1}{\overline{g_1''\zeta_{1,0}^2}} \times \left[2U\zeta_{1,0} + \mathrm{i}\omega\overline{r_1''\zeta_{1,0}^2} + \overline{u_{\eta,0}'\zeta_{1,0}^2}\dot{\eta}_c + \overline{u_{a,0}'\zeta_{1,0}^2}\dot{a} + \sum_{n=2}^{N} \frac{\mathrm{i}\Gamma_n}{2\pi} \times \left(\frac{\zeta_n^2 \bar{\zeta}_{1,0}^2}{(\zeta_n\bar{\zeta}_{1,0} - r_c^2)^2} - \frac{\bar{\zeta}_{1,0}^2}{(\bar{\zeta}_{1,0} - \bar{\zeta}_n)^2} \right) \right]. \tag{A.2}$$

Subtracting a slight variation of (A.1) from the quantity inside the brackets of (A.2) produces the following equation:

$$\begin{aligned} r_c^4 |g_1''|^2 \left(\epsilon\dot{\epsilon} + \frac{5\epsilon^2}{4\tau}\right) = {} & 2Re\left(U\zeta_{1,0}\right) \\ & + \mathrm{i}\omega\overline{[r_1'\zeta_{1,0} - \bar{g}_1 g_1''\zeta_{1,0}^2 + r_1''\zeta_{1,0}^2]} \\ & + \overline{(u_{\eta,0}\zeta_{1,0} + u_{\eta,0}'\zeta_{1,0}^2)}\dot{\eta}_c \\ & + \overline{(u_{a,0}\zeta_{1,0} + u_{a,0}'\zeta_{1,0}^2 - 2g_1''\zeta_{1,0}^2)}\dot{a} \\ & - \sum_{n=2}^{N} \frac{\Gamma_n}{\pi} Im\left(\frac{\zeta_n\zeta_{1,0}}{(\zeta_n - \zeta_{1,0})^2}\right) \end{aligned} \tag{A.3}$$

which is integrated for ϵ as $\epsilon^2 = C\tau$ where:

$$\begin{aligned} C = {} & \frac{a^2}{7r_c^4} \Bigg[2Re\left(U\zeta_{1,0}\right) + \mathrm{i}\omega\overline{(r_1'\zeta_{1,0} + r_1''\zeta_{1,0}^2 - \bar{g}_1 g_1''\zeta_{1,0}^2)} \\ & + \overline{(u_{\eta,0}\zeta_{1,0} + u_{\eta,0}'\zeta_{1,0}^2)}\dot{\eta}_c \\ & + \overline{(u_{a,0}\zeta_{1,0} + u_{a,0}'\zeta_{1,0}^2 - 2g_1''\zeta_{1,0}^2)}\dot{a} \\ & - \sum_{n=2}^{N} \frac{\Gamma_n}{\pi} Im\left(\frac{\zeta_n\zeta_{1,0}}{(\zeta_n - \zeta_{1,0})^2}\right) \Bigg]. \end{aligned} \tag{A.4}$$

Further computation shows that all terms in C are real and given by

$$\begin{aligned} & r_1'\zeta_{1,0} - \bar{g}_1 g_1''\zeta_{1,0}^2 + r_1''\zeta_{1,0}^2 = 2\mathrm{i}\eta_c\left(3a + \frac{\xi_c^2 + \eta_c^2}{a - 2\xi_c}\right), \\ & u_{\eta,0}\zeta_{1,0} + u_{\eta,0}'\zeta_{1,0}^2 \\ & \quad = -\frac{2r_c^2\eta_c}{a(a-2\xi_c)^2}\left(3a - 4\xi_c + \frac{2(\xi_c^2 + \eta_c^2)}{a - 2\xi_c}\right), \\ & u_{a,0}\zeta_{1,0} + u_{a,0}'\zeta_{1,0}^2 - 2g_1''\zeta_{1,0}^2 \\ & \quad = -4\left(a - \xi_c + \frac{3\eta_c^2}{a} + \frac{2\xi_c^2}{a - 2\xi_c} - \frac{(a-\xi_c)(\xi_c^3 - a\eta_c^2)}{(a-2\xi_c)^2}\right). \end{aligned} \tag{A.5}$$

References

[1] M. Hultmark, M. Leftwich, A.J. Smits, Flowfield measurements in the wake of a robotic lamprey, Exp Fluids. 43 (5) (2007) 683–690.
[2] E.D. Tytell, G.V. Lauder, The hydrodynamics of eel swimming: I. Wake structure, J. Exp. Biol. 207 (2004) 1825–1841.
[3] Q. Zhu, M.J. Wolfgang, D.K.P. Yue, M.S. Triantafyllou, Three-dimensional flow structures and vorticity control in fish-like swimming, J. Fluid Mech. 468 (2002) 1–28.
[4] G.R. Spedding, A.H. Hedenström, J. McArthur, M. Rosén, The implications of low-speed fixed-wing aerofoil measurements on the analysis and performance of flapping bird wings, J. Exp. Biol. 211 (2008) 215–223.
[5] J.M. Anderson, K. Streitlien, D.S. Barrett, M.S. Triantafyllou, Oscillating foils of high propulsive efficiency, J. Fluid Mech. 360 (1998) 4172.
[6] J.H.J. Buchholz, A.J. Smits, The wake structure and thrust performance of a rigid low-aspect-ratio pitching panel, J. Fluid Mech. 603 (2008) 331–365.
[7] M.M. Koochesfahani, Vortical patterns in the wake of an oscillating airfoil, AIAA J. 27 (1989) 1200–1205.
[8] T. Schnipper, A. Andersen, T. Bohr, Vortex wakes of a flapping foil, J. Fluid Mech. 633 (2009) 411–423.
[9] M.S. Triantafyllou, G.S. Triantafyllou, R. Gopalkrishnan, Wake mechanics for thrust generation in oscillating foils, Phys. Fluids A 3 (12) (1991) 2835–2837.
[10] C.H.K. Williamson, A. Roshko, Vortex formation in the wake of an oscillating cylinder, J. Fluid. Struct. 2 (1988) 355–381.
[11] T. Wu, Swimming of a waving plate, J. Fluid Mech. 10 (1961) 321–344.
[12] J. Lighthill, Mathematical Biofluiddynamics, Society for Industrial and Applied Mathematics, PA, 1975.
[13] S. Childress, Mechanics of Swimming and Flying, Cambridge University Press, 1981.
[14] D. Weihs, A hydrodynamical analysis of fish turning manoeuvres, Proc. R. Soc. Lond. B 182 (1972) 59–72.
[15] D. Weihs, The mechanism of rapid starting of slender fish, Biorheology 10 (1973) 343–350.
[16] E. Kanso, Swimming due to transverse shape deformations, J. Fluid Mech. 631 (2009) 127–148.
[17] S. Kelly, H. Xiong, Self-propulsion of a free hydrofoil with localized discrete vortex shedding: analytical modeling and simulation, Theor. Comput. Fluid Dyn. 24 (2010) 45–50.
[18] R. Mason, 2003, Fluid locomotion and trajectory planning for shape-changing robots. Ph.D. Thesis, California Institute of Technology, Pasadena, CA.
[19] M.A. Jones, The separated flow of an inviscid fluid around a moving flat plate, J. Fluid Mech. 496 (2003) 405–441.
[20] M. Nitsche, R. Krasny, A numerical study of vortex ring formation at the edge of a circular tube, J. Fluid Mech. 216 (1994) 139–161.
[21] R.K. Shukla, J.E. Eldredge, An inviscid model for vortex shedding from a deforming body, Theor. Comput. Fluid Dyn. 21 (5) (2007) 343–368.
[22] I. Borazjani, F. Sotiropoulos, Numerical investigation of the hydrodynamics of anguilliform swimming in the transitional and inertial flow regimes, J. Exp. Biol. 212 (2009) 576–592.
[23] J.D. Eldredge, Dynamically coupled fluid-body interactions in vorticity-based numerical simulations, J. Comput. Phys. 227 (2008) 9170–9194.
[24] S. Kern, P. Koumoutsakos, Simulations of optimized anguilliform swimming, J. Exp. Biol. 209 (2006) 4841–4857.
[25] L. Cortelezzi, A. Leonard, Point vortex model of the unsteady separated flow past a semi-infinite plate with transverse motion, Fluid Dyn. Res. 11 (1993) 263–295.
[26] S. Michelin, S.G. Llewellyn Smith, An unsteady point vortex method for coupled fluid–solid problems, Theor. Comput. Fluid Dyn. 23 (2009) 127–153.
[27] J.X. Sheng, A. Ysasi, D. Kolomenskiy, E. Kanso, M. Nitsche, K. Schneider, 2010, Simulating vortex wakes of flapping plates, IMA Volume on Natural Locomotion in Fluids and on Surfaces: Swimming, Flying, and Sliding, preprint.
[28] P.K. Newton, The *N*-Vortex problem: analytical techniques, Appl. Math. Sci. 145 (2001).
[29] A.V. Borisov, I.S. Mamaev, An integrability of the problem on motion of cylinder and vortex in the ideal fluid, Regul. Chaotic Dyn. 8 (2003) 163–166.
[30] E. Kanso, B. Oskouei, Stability of a coupled body-vortex system, J. Fluid Mech. 800 (2008) 77–94.
[31] J. Roenby, H. Aref, Chaos in body-vortex interactions, Proc. R. Soc. Lond. A 466 (2010) 1871–1891.
[32] B.N. Shashikanth, J.E. Marsden, J.W. Burdick, S.D. Kelly, The Hamiltonian structure of a 2D rigid circular cylinder interacting dynamically with *N* Point vortices, Phys. Fluids 14 (3) (2002) 1214–1227. (see also Erratum, Phys. Fluids 14 (11) 4099).
[33] E. Kanso, J.E. Marsden, C.W. Rowley, J. Melli-Huber, Locomotion of articulated bodies in a perfect fluid, J. Nonlinear Sci. 15 (2005) 255–289.
[34] H. Lamb, Hydrodynamics, sixth ed., Dover, NY, 1932.
[35] N.I. Muskhelishvili, Singular Integral Equations, Noordhoff, Groningen, Holland, 1953.
[36] D.G. Crowdy, A. Surana, K.-Y Yick, The irrotational flow generated by two planar stirrers in inviscid fluid, Phys. Fluids 19 (2007) 018103.
[37] P.G. Saffman, 1992, Vortex dynamics, Cambridge Monographs on Mechanics and Applied Mathematics.
[38] C.C. Lin, On the motion of vortices in two-dimensions—I. existence of the Kirchhoff–Routh function, Proc. N. A. S. 27 (1941) 570–575.
[39] C.C. Lin, On the motion of vortices in two-dimensions—II. some further investigations on the Kirchhoff–Routh function, Proc. N. A. S. 27 (1941) 575–577.
[40] L. Cortelezzi, Y.C. Chen, H.L. Chang, Nonlinear feedback control of the wake past a plate: from a low-order model to a higher-order model, Phys. Fluids 9 (1997) 2009–2022.
[41] F.L. Ponta, H. Aref, Vortex synchronization regions in shedding from an oscillating cylinder, Phys. Fluids 17 (2005) 011703.